

Directed flow in Au+Au, Xe+CsI and Ni+Ni collisions and the nuclear equation of state

A. Andronic⁴, W. Reisdorf⁴, N. Herrmann⁶, P. Crochet³, J.P. Alard³, V. Barret³, Z. Basrak¹², N. Bastid³, G. Berek², R. Čaplar¹², A. Devismes⁴, P. Dupieux³, M. Dželalija¹², C. Finck⁴, Z. Fodor², A. Gobbi⁴, Yu. Grishkin⁷, O.N. Hartmann⁴, K.D. Hildenbrand⁴, B. Hong⁹, J. Kecskemeti², Y.J. Kim⁹, M. Kirejczyk¹¹, P. Koczon⁴, M. Korolija¹², R. Kotte⁵, T. Kress⁴, A. Lebedev⁷, Y. Leifels⁴, X. Lopez³, M. Merschmeyer⁶, W. Neubert⁵, D. Pelte⁶, M. Petrovici¹, F. Rami¹⁰, B. de Schauenburg¹⁰, A. Schüttauf⁴, Z. Seres², B. Sikora¹¹, K.S. Sim⁹, V. Simion¹, K. Siwek-Wilczyńska¹¹, V. Smolyankin⁷, M.R. Stockmeier⁶, G. Stoicea¹, Z. Tymiński^{4,11}, P. Wagner¹⁰, K. Wiśniewski¹¹, D. Wohlfarth⁵, I. Yushmanov⁸, A. Zhilin⁷

(FOPI Collaboration)

¹ National Institute for Physics and Nuclear Engineering, Bucharest, Romania

² KFKI Research Institute for Particle and Nuclear Physics, Budapest, Hungary

³ Laboratoire de Physique Corpusculaire, IN2P3/CNRS, and Université Blaise Pascal, Clermont-Ferrand, France

⁴ Gesellschaft für Schwerionenforschung, Darmstadt, Germany

⁵ Forschungszentrum Rossendorf, Dresden, Germany

⁶ Physikalisches Institut der Universität Heidelberg, Heidelberg, Germany

⁷ Institute for Theoretical and Experimental Physics, Moscow, Russia

⁸ Kurchatov Institute, Moscow, Russia

⁹ Korea University, Seoul, South Korea

¹⁰ Institut de Recherches Subatomiques, IN2P3-CNRS, Université Louis Pasteur, Strasbourg, France

¹¹ Institute of Experimental Physics, Warsaw University, Poland

¹² Rudjer Boskovic Institute, Zagreb, Croatia

We present new experimental data on directed flow in collisions of Au+Au, Xe+CsI and Ni+Ni at incident energies from 90 to 400A MeV. We study the centrality and system dependence of integral and differential directed flow for particles selected according to charge. All the features of the experimental data are compared with Isospin Quantum Molecular Dynamics (IQMD) model calculations in an attempt to extract information about the nuclear matter equation of state (EoS). We show that the combination of rapidity and transverse momentum analysis of directed flow allow to disentangle various parametrizations in the model. At 400A MeV, a soft EoS with momentum dependent interactions is best suited to explain the experimental data in Au+Au and Xe+CsI, but in case of Ni+Ni the model underpredicts flow for any EoS. At 90A MeV incident beam energy, none of the IQMD parametrizations studied here is able to consistently explain the experimental data.

PACS: 25.70.Lm, 21.65.+f, 25.75.Ld

I. INTRODUCTION

The study of collective flow in relativistic heavy-ion collisions has been an intense field of research for the past twenty years (see Refs. [1,2] for recent reviews). The ultimate motivation for the whole endeavour has been the extraction of the equation of state (EoS) of nuclear matter (see Ref. [3] for an early account and Ref. [4] for more recent ones). Moreover, the study of highly complex (quantum) many-body dynamics of heavy-ion collisions is in itself a challenging task.

The (in-plane) directed (or sideward) flow was pre-

dicted for semi-central heavy-ion collisions on the basis of fluid dynamical calculations [5] and observed in experiments soon after [6,7]. The study of the average in-plane transverse momentum, $\langle p_x \rangle$, as a function of rapidity, y , provides an easy and intuitive way of quantizing the directed flow [8]. For beam energy range up to a few GeV per nucleon, the experimental [8–24] and theoretical [25–43] studies of this phenomenon have provided important understanding of its features. Experimentally, the dependences of directed flow on incident energy [9,16,19,18,22], centrality [9,15,17,19–22], particle type [10,16,17,19–22], system size [9,18,22] and isospin [21] have been determined. These main features have been quantitatively reproduced by microscopic transport models of either Quantum Molecular Dynamics (QMD) [29,33,15,16,20,41,24] or Boltzmann-Uehling-Uhlenbeck (BUU) [11,30,31,36,38,17,40,42,43,24] type. Despite all these efforts, a definite conclusion on the EoS has not yet been achieved. As pointed out early on [27,31,32], the momentum dependent interactions (MDI) play a crucial role in the determination of the EoS. The directed flow is influenced in addition by the (in-medium) nucleon-nucleon cross section (σ_{nn}) [36,37,44]. Moreover, consistency is needed in deriving EoS together with both MDI and σ_{nn} [35,43]. The importance to combine various observables, each sensitive (ideally) to one particular aspect of the parameters that influence EoS was emphasized recently [4].

The results quoted above have been obtained from the analysis of integrated directed flow. The first analysis of differential directed flow (DDF) was introduced by Pan and Danielewicz [36], who studied the transverse momentum (p_t) dependence of the first order Fourier coefficient,

$v_1 = \langle \cos(\phi) \rangle$, where ϕ is the angle with respect to the reaction plane. The DDF was studied around the balance energy (E_{bal} , which is the energy of disappearance of flow [14,16,23]) by Li and Sustich [44], who unraveled its interesting patterns. They also pointed out the marked sensitivity of DDF to both EoS and nucleon-nucleon cross section (σ_{nn}). At AGS energies the DDF was studied both experimentally [45] and theoretically [46,47]. Recently, we have completed the first experimental analysis of DDF for Au+Au collisions at incident energies from 90 to 400 A MeV [48]. We have found interesting patterns of the differential flow, evolving as a function of incident energy, particle type and rapidity. In particular, the study of high- p_t particles is important because, as proposed in Ref. [49], they are good messengers from the high density state of the collision. The DDF could additionally provide snapshots of the flow development during the time of the collision.

In this paper we present new experimental data on directed flow in collisions of Au+Au, Xe+CsI and Ni+Ni. The complete coverage of the FOPI detector makes possible precision studies of flow, refining our earlier studies done with Phase I data [15,19,20,22]. Following our recent exploration of the energy range of 90 to 400 A MeV for Au+Au [48], we focus here on the centrality (for Au+Au) and on system size dependence of directed flow. This analysis has been performed for the incident energies of 250 and 400 A MeV, for particles with $Z=1$ and $Z=2$. To avoid overloading, only a selection of results is included in the body of the paper. In the Appendix we provide additional figures to complete the data set. After describing the detector, the method of analysis, and the corrections applied to data, we study the centrality and system dependence of directed flow over the complete forward rapidity range, both in terms of (p_t) integrated and in a differential way. All the features of the experimental data are then compared with IQMD model calculations for the incident energies of 90 and 400 A MeV.

II. SET-UP AND DATA ANALYSIS

The data have been measured with a wide phase-space coverage using the FOPI detector [50] at GSI Darmstadt. The reaction products are identified by charge (Z) in the forward Plastic Wall (PW) at $1.2^\circ < \theta_{lab} < 30^\circ$ using time-of-flight (ToF) and specific energy loss. In the Central Drift Chamber (CDC), covering $34^\circ < \theta_{lab} < 145^\circ$, the particle identification is on mass (mass number A), obtained using magnetic rigidity and the energy loss. For PW the Z resolution is 0.13 charge units for $Z=1$ and 0.14 for $Z=2$, while for CDC the mass resolution varies from 0.20 to 0.53 mass units for $A=1$ to $A=4$. The contamination of $Z=1$ in the $Z=2$ sample varies from 6% to 10% (from Ni+Ni at 250 A MeV to Au+Au at 400 A MeV) for the PW and is up to 20% for the CDC (where it is the contamination of $A=1,2$ and 3 in the $A=4$ sam-

ple). The PW measures the velocity of particles via ToF with an average resolution of 150 ps. For the CDC, the relative momentum resolution σ_{p_t}/p_t varies from 4% for $p_t < 0.5$ GeV/c to about 12% for $p_t=2$ GeV/c. For more details on the detector configuration for this experiment see Ref. [51].

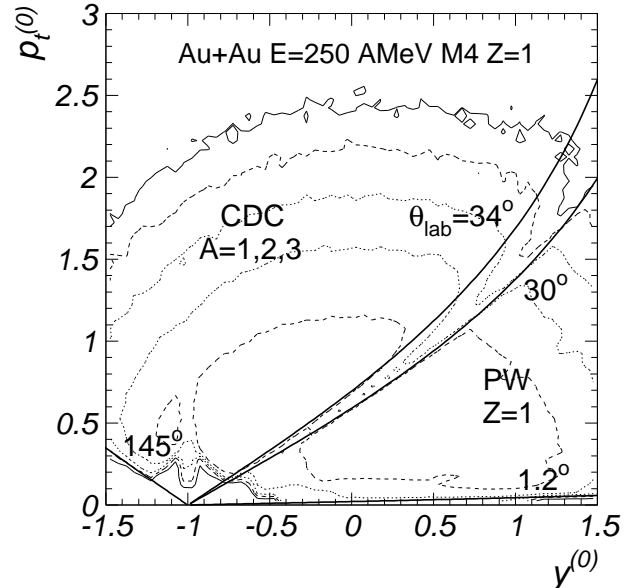


FIG. 1. FOPI detector acceptance: phase-space distribution for $Z=1$ particles measured in the centrality bin M4 of the reaction Au+Au at 250 A MeV. The intensity contours are spaced logarithmically. The thicker lines mark the geometrical acceptance of different subdetectors.

The phase-space coverage of the FOPI detector is presented in Fig. 1 for particles with $Z=1$ (for PW) and $A=1,2,3$ (for CDC), measured in semi-central collisions Au+Au at incident energy of 250 A MeV. To compare different incident energies and particle species, we use normalized center-of-mass (c.m.) transverse momentum (per nucleon) and rapidity, defined as

$$p_t^{(0)} = (p_t/A)/(p_P^{c.m.}/A_P), \quad y^{(0)} = (y/y_P)^{c.m.},$$

where the subscript P denotes the projectile. For the PW coverage, shadows around $\theta_{lab} = 7^\circ$ and 19° are visible, arising from subdetector borders and frames.

For the centrality selection we used the charged particle multiplicities, classified into five bins, M1 to M5. The variable $E_{rat} = \sum_i E_{\perp,i} / \sum_i E_{\parallel,i}$ (the sums run over the transverse and longitudinal c.m. kinetic energy components of all the products detected in an event) has been additionally used for a better selection of the most central collisions (M5 centrality bin). The geometric impact parameters interval for the centrality bins M3, M4, and M5 for Au+Au system at 400 A MeV studied here are presented in Table I.

The impact parameter intervals corresponding to the three investigated systems at the incident energy of

TABLE I. The geometric impact parameters intervals Δb_{geo} and the correction factors for the reaction plane resolution, $1/\langle \cos \Delta\phi \rangle$, for three centrality bins of Au+Au collisions at the incident energy of 400A MeV.

Centrality bin	M3	M4	M5
Δb_{geo} (fm)	6.1-7.6	1.9-6.1	0-1.9
$1/\langle \cos \Delta\phi \rangle$	1.05	1.04	1.17

TABLE II. The geometric impact parameters intervals Δb_{geo} , the reduced impact parameters $\langle b_{geo} \rangle / b_{geo}^{max}$ and the correction factors for the reaction plane resolution, $1/\langle \cos \Delta\phi \rangle$, for the three systems at the incident energy of 250A MeV, M4 centrality bin.

System	Au+Au	Xe+CsI	Ni+Ni
Δb_{geo} (fm)	1.9-6.1	1.7-4.8	1.5-3.4
$\langle b_{geo} \rangle / b_{geo}^{max}$	0.31	0.29	0.27
$1/\langle \cos \Delta\phi \rangle$	1.05	1.09	1.27

250A MeV, M4 centrality bin, are presented in Table II along with the reduced impact parameters $\langle b_{geo} \rangle / b_{geo}^{max}$. b_{geo}^{max} is the maximum geometrical impact parameter, calculated as: $b_{geo}^{max} = 1.2(A_P^{1/3} + A_T^{1/3})$ (in fm). Applying the same recipe for the centrality selection for different systems the reduced impact parameter is similar, as seen in Table II.

The largest data sample was acquired with what we call ‘‘Medium bias’’ trigger, which accepts events roughly corresponding to centrality bins M3, M4 and M5 for Au+Au collisions. For Xe and Ni systems this trigger selection amounts to a bias for the M3 centrality. This is the reason why M3 is not included in the present paper for these systems. We have collected ‘‘Minimum bias’’ data for all systems, but the statistics is far smaller, thus not allowing the type of analysis done in this paper.

A. The reaction plane determination and the correction for its resolution

The reaction plane has been reconstructed event-by-event using the transverse momentum method [8]. All charged particles detected in an event have been used, except a window around midrapidity ($|y^{(0)}| < 0.3$) to improve the resolution. The particle-of-interest has been excluded to prevent autocorrelations.

The correction of the extracted values due to the reconstructed reaction plane fluctuations has been done using the recipe of Ollitrault [52]. The resolution of the reaction plane azimuth, $\Delta\phi$, can be extracted by randomly dividing each event in two subevents and calculating for each one the reaction plane orientation, Φ_1 and Φ_2 [8,52]. From the resolution, quantified as $\langle \cos(\Phi_1 - \Phi_2) \rangle$, the correction factors, $1/\langle \cos \Delta\phi \rangle$ can be calculated [52] (see Ref. [51] for more technical details). For the experimental data the correction factors for the centrality bins M3,

M4, and M5 for Au+Au system at 400A MeV are presented in Table I. The values for the three investigated systems at the incident energy of 250A MeV, M4 centrality bin, are presented in Table II.

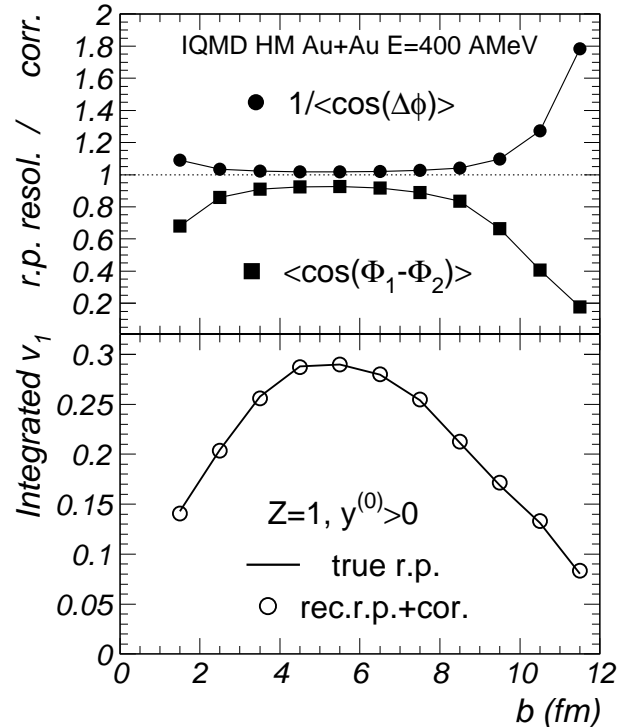


FIG. 2. Upper panel: the resolution of the reconstructed reaction plane (squares) and the corresponding correction factors (dots). Lower panel: v_1 values for the true (continuous line) and reconstructed and corrected (dashed line) reaction plane. IQMD HM events were used for these studies.

The accuracy of the reaction plane correction procedure was checked using Isospin Quantum Molecular Dynamics (IQMD) [33] events analyzed in the same way as the data. The results are shown in Fig. 2 for IQMD events at 400A MeV. The upper panel presents the resolution and the correction factor as a function of the impact parameter, b . Their dependence on centrality reflects mainly the dependence of the strength of the directed flow (see lower panel), but also a finite number effect [8], evident towards peripheral collisions. The lower panel of Fig. 2 presents the centrality dependence of integrated v_1 values for $Z=1$ particles (for the forward hemisphere), derived from IQMD events in two cases: i) with respect to the true reaction plane (known in the model) and ii) with respect to the reconstructed reaction plane and using the correction according to [52] (correction factors of the upper panel of Fig. 2). The agreement between the two cases is perfect, down to most peripheral collisions, where correction factors up to 2 are necessary.

Alternative methods of flow analysis have been proposed recently [53]. However, because, for our energy domain, the flow of nucleons is at its maximum and pro-

duced particles are very rare, the impact of these refined methods is expected to be minor.

B. The influence of FOPI detector on the flow measurements

As seen in Fig. 1, the complete phase space coverage of the FOPI detector (in its Phase II) is hampered by one empty region, corresponding to polar angles θ_{lab} from 30° to 34° in the laboratory frame. Additional detector shadows around 7° and 19° are present too. We have studied the effect of the FOPI acceptance using IQMD transport model [33]. The IQMD events were analyzed in the same way as the experimental data.

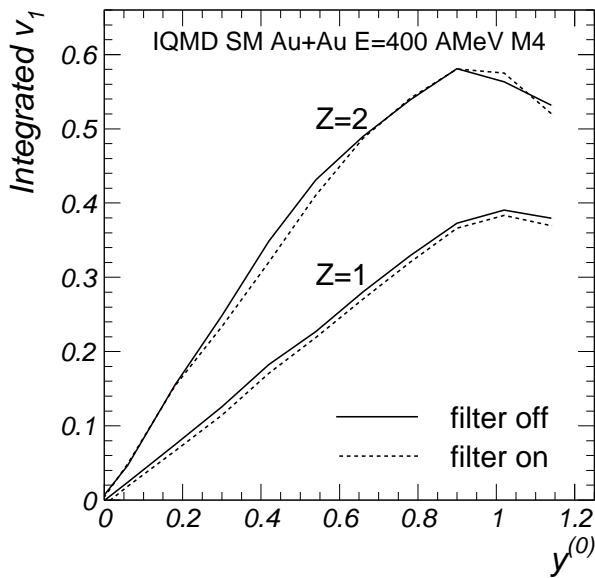


FIG. 3. The effect of the FOPI detector filter on v_1 values for $Z=1$ and $Z=2$ particles for the incident energy of 400A MeV, M4 centrality bin. IQMD SM events were used for this comparison.

The results are presented in Fig. 3, where the integrated v_1 values as a function of rapidity for $Z=1$ and $Z=2$ particles are shown for the ideal case of total coverage (full lines) and when the FOPI filter is employed (dashed lines). IQMD SM events for the incident energy of 400A MeV, M4 centrality bin were used for this comparison. With the present configuration of the detector, the measured v_1 values are very close to the ideal case. We note that, for our published directed flow data [15,19,20,22], although the effect of the FOPI acceptance on the directed flow results was quite small [15,54], its magnitude was comparable to the difference between soft and hard EoS.

An important ingredient in the present analysis is the correction for distortions due to multiple hit losses. As an example, in case of PW, despite its good granularity (512

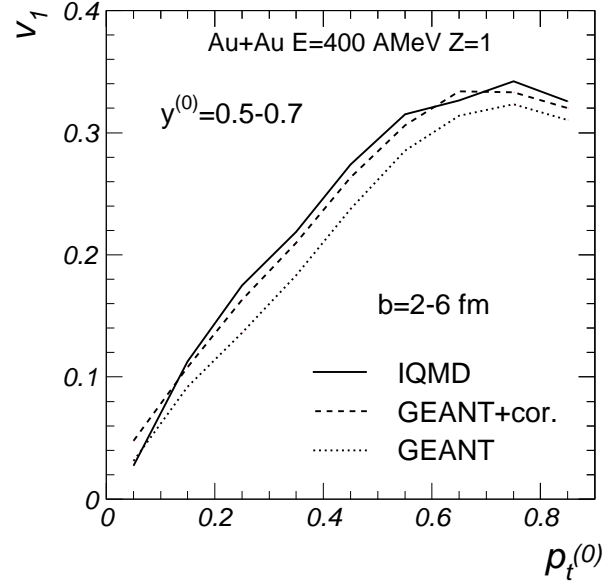


FIG. 4. The effect of the FOPI detector on v_1 values for $Z=1$ particles, for the incident energy of 400A MeV, M4 centrality bin. IQMD events were used for this comparison. Three cases are compared: the simple geometric FOPI filter (full line) and GEANT simulation without (dotted line) and with (dashed line) the multiple hit correction.

independent modules [50]), average multiple hit probabilities of up to about 9% at 400A MeV are registered for the multiplicity bin M4. Because of the directed flow, the average number of particles detected over the full PW subdetector is up to 2 times higher in-plane than out of the reaction plane. As a consequence, the losses due to multiple hit are strongly correlated with the directed flow and follow its dependences on incident energy, centrality and system size. These losses lead to an underestimation of the measured directed flow and need to be taken into account. We developed a correction procedure based on the experimental data, by exploiting the DDF left-right symmetry with respect to midrapidity. The correction acts upon v_1 values (namely only on average values) and is deduced for each system, energy and centrality separately. Due to the flow profile in the polar angle, it depends also on transverse momentum. It is larger for $Z=2$ compared to $Z=1$ particles. The correction was derived in a window around midrapidity ($|y^{(0)}| < 0.1$) and propagated for other rapidity windows for each $p_t^{(0)}$ bin along the lines of constant θ_{lab} to follow the detector segmentation. It reaches up to 12% for Au+Au at 400A MeV and is almost negligible at 90A MeV. At 400A MeV it is up to 5% for Xe+CsI and up to 2% for Ni+Ni.

The procedure was checked and validated using IQMD events passed through a complete GEANT [55] simulation of the detector. IQMD events were used for this study, at the incident energy of 400A MeV. The results are presented in Fig. 4 for $Z=1$ particles in M4 central-

ity bin. The v_1 values extracted from IQMD events as inputs into a complete GEANT simulation of the detector (and analyzed in exactly the same way as the data), without (dotted line) and with (dashed line) the multiple hit correction, are compared with the true v_1 values, obtained from standard IQMD events (actually the same events used for the GEANT simulation) with only a simple geometric FOPI filter (full line). It is obvious that the correction is restoring the “true” v_1 values (IQMD) from the “measured” GEANT values. Also, the correction used for the data is quantitatively reproduced by these simulations. Note that, because of larger multiplicities for $Z=1$ particles from IQMD (see Section IV), the correction is larger in the simulations than in the data. As a result of these studies, all the experimental data (both differential and integrated) have been corrected according to the procedure described above.

The only source of systematic error on our measured v_1 values could be the correction for multiple hit losses outlined above. However, as we have demonstrated based on complete GEANT simulations, this correction is well understood. As a result, the systematic error depends on incident energy, centrality, particle type and $p_t^{(0)}$. It is below 5% on the differential v_1 . There are exceptions for some points, for which the systematic error arises from (rapidity-dependent) regions in $p_t^{(0)}$ in which detector shadows are influencing the data. For those particular points the systematic error is already included in the plots. For the integrated v_1 values the error is slightly smaller, up to 4%, including the influence of the uncovered region of $\theta_{lab} = 30^\circ - 34^\circ$. These values do not include the effect of particle misidentification.

III. GENERAL FEATURES OF THE DATA

A. Centrality dependence

By varying the centrality of the collision one aims at controlling both the size of the participant fireball (and consequently the magnitude of the achieved compression and subsequent expansion) and the size of the spectator fragment region. While semi-central collisions could provide information preferentially on (density dependent) EoS, more peripheral reactions can help in pinning down the MDI [4].

Figure 5 shows the centrality dependence of the directed flow for Au+Au at 400A MeV for $Z=2$ particles. Plotted as a function of rapidity are the $\langle p_t \rangle$ integrated v_1 values (upper panel) and those integrated values weighted by the average transverse momentum, $\langle p_t^{(0)} \rangle$, for the respective rapidity bin. This weighted v_1 quantity is proportional to the average in-plane transverse momentum $\langle p_x \rangle$ ($v_1 = \langle p_x / p_t \rangle$) and was chosen due to its convenience in applying the corrections discussed in Section II B. First, one can notice that the known

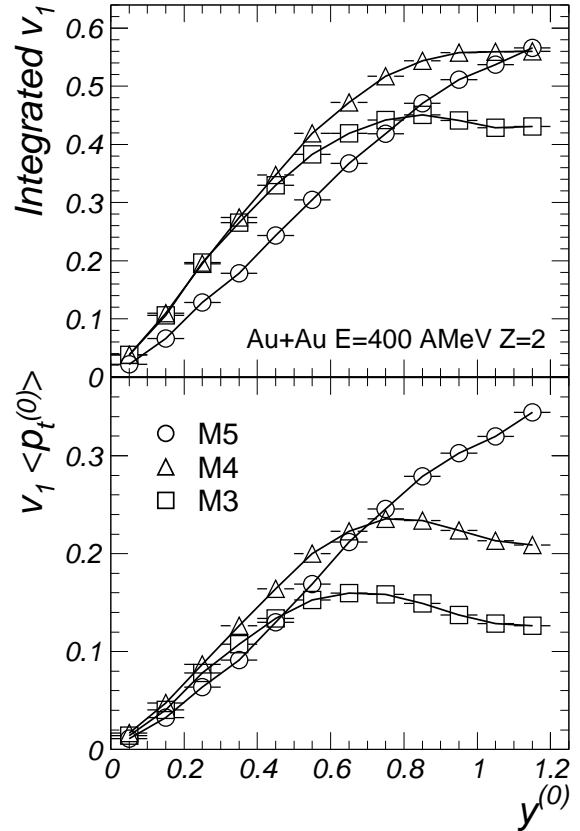


FIG. 5. Centrality dependence of the integrated directed flow as a function of rapidity for Au+Au at 400A MeV for $Z=2$ particles. The lines are joining the symbols to guide the eye.

behaviour of the slope at midrapidity, namely the maximum for intermediate impact parameters (M4 bin), is evident only for the weighted v_1 values (lower panel of Fig. 5). The asymmetries (v_1 values, upper panel) are the same around midrapidity for M3 and M4 centrality bins. Second, in both observables, the most significant dependence on centrality is taking place in the spectator region (roughly $y^{(0)} > 0.5$) and it is more pronounced for the weighted v_1 values. Both the asymmetries and the in-plane transverse momentum reflect the influence of the participant and of the spectator size controlled by the variation of the centrality. These distributions are inherently a result of the superposition of collective and thermal contributions [22]. For a given flow magnitude, higher temperatures (presumably achieved for more central collision) would translate into a smaller effective flow.

In Fig. 6 we show the centrality dependence of the differential flow for $Z=2$ particles for Au+Au collisions at 400A MeV. Three centrality bins (different panels) are compared for three rapidity windows (different symbols). The lines are polynomial fits to guide the eye. The rapidity dependence of the DDF in different centrality bins follows the rapidity dependence of the integrated flow

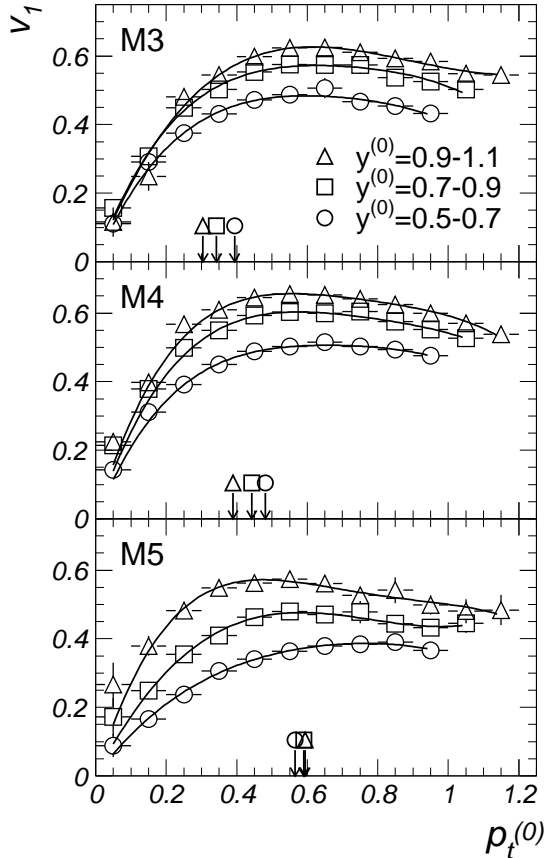


FIG. 6. Differential flow for three centrality bins, in three rapidity windows, for $Z=2$ particles for collisions Au+Au at 400A MeV. The lines are polynomial fits to guide the eye. The arrows mark the values of the average $p_t^{(0)}$ for the corresponding centrality bin.

seen in Fig. 5: the most pronounced dependence is registered for the most central collisions, M5. As we have already discussed in [48], the shape of the DDF (a gradual development of a limiting value, followed by a decrease at high $p_t^{(0)}$) could be a result of the collision dynamics. Part of the high- p_t particles could have been emitted at a pre-equilibrium stage, therefore not reaching the maximum compression stage of the reaction. However, this possibility seems to be ruled out by the observation that the high- p_t particles originate preferentially from high-density regions of the collision [49].

The arrows in Fig. 6 mark the values of the average $p_t^{(0)}$ for the corresponding centrality bin, according to the symbols. For this incident energy of 400A MeV the value of the projectile momentum in the c.m. system is 433 MeV/c per nucleon. Higher values of average transverse momenta are seen for more central collisions as a result of a stronger expansion from a bigger and more compressed source. The dependence of $\langle p_t^{(0)} \rangle$ on rapidity is different for the most central collisions (M5 bin) compared to semi-central ones, for which smaller transverse

momenta are seen towards the projectile rapidity as a result of the influence of the spectator matter.

Similar data as those presented in Fig. 5 and 6 are presented in the Appendix for $Z=1$ particles in Au+Au at 400A MeV and for $Z=1$ and $Z=2$ particles at 250A MeV (Fig. 19 to Fig. 24).

B. System size dependence

As for the centrality variation, by varying the system size one aims to control the size of both the participant and the spectator. However, the question whether transparency plays a role in case of lighter systems, needs to be addressed simultaneously, as it results in a decrease of the achieved compression. In addition, the surface (or surface-to-volume ratio) can play an important role. It was suggested that the system size dependence of the directed flow could give insights about σ_{nn} [32].

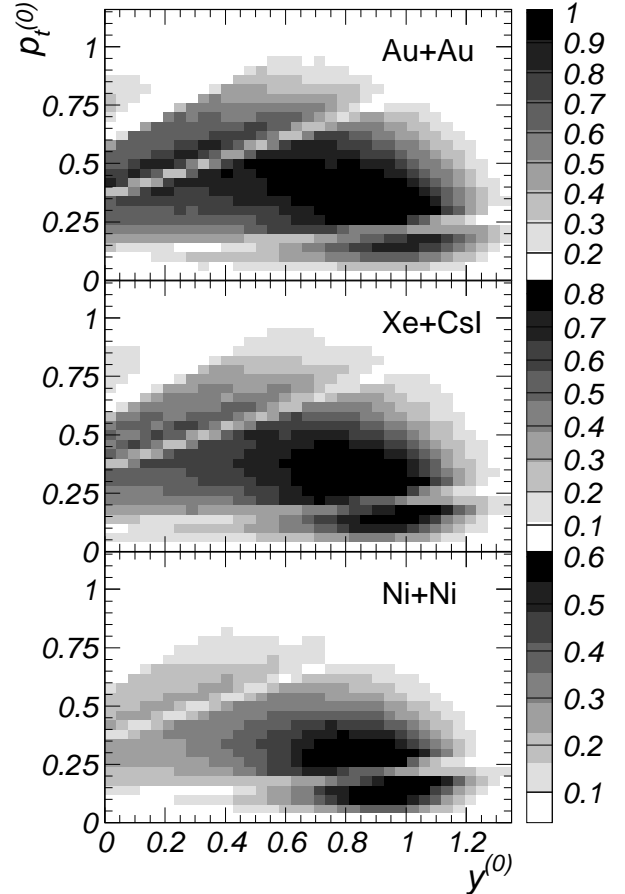


FIG. 7. Phase space distributions $d^2N/dp_t^{(0)} dy^{(0)}$ of $Z=2$ particles for three systems at the incident energy of 250A MeV, M4 centrality.

Figure 7 presents the phase space distribution $d^2N/dp_t^{(0)} dy^{(0)}$ of $Z=2$ particles for the three systems

at the incident energy of 250A MeV, centrality bin M4. From Au+Au to Ni+Ni system, the phase space population becomes more and more focused, both in transverse momentum and rapidity. This is an indication of the decrease of stopping for lighter systems. Maximum density reached in the fireball depends on the system size [34], presumably as an effect of different stopping. On the other hand, due to the sizes of both fireball and spectator, the separation between the two regions is clearer (smaller surface contacts) for lighter systems.

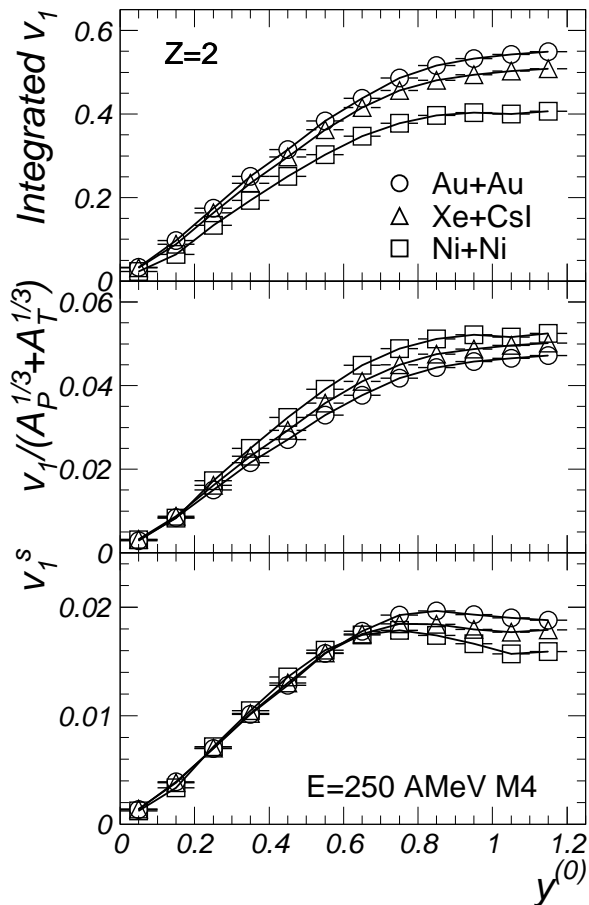


FIG. 8. Integrated directed flow as a function of rapidity for $Z=2$ particles in the M4 centrality bin of collisions Au+Au, Xe+CsI and Ni+Ni at 250A MeV. Upper panel: v_1 values, middle panel: v_1 scaled by the term $(A_P^{1/3} + A_T^{1/3})$, lower panel: scaled values, v_1^s (see text). The lines are joining the symbols to guide the eye.

Figure 8 shows the system dependence of the directed flow for $Z=2$ particles in the M4 centrality bin of collisions Au+Au, Xe+CsI and Ni+Ni at 250A MeV. Plotted are the integrated v_1 values as a function of rapidity for three cases: i) as such (upper panel); ii) scaled with the term $(A_P^{1/3} + A_T^{1/3})$, which is proportional to the sum of radii of projectile and target (middle panel); iii) scaled as: $v_1^s = v_1 \langle p_t^{(0)} \rangle / (A_P^{1/3} + A_T^{1/3})$, where $\langle p_t^{(0)} \rangle$ is the average

normalized transverse momentum for each rapidity bin. It is evident that for the first two cases there is no scaling with respect to the system size, neither without nor with accounting for the system size via the $(A_P^{1/3} + A_T^{1/3})$ term, while the in-plane average transverse momenta, proportional to v_1^s , shows system size scaling (lower panel of Fig. 8) for the participant region. Somewhat expected, a deviation is present for the spectator part. We have observed a very similar feature for $Z=3$ particles, while for $Z=1$ the scaling holds over all the forward rapidity domain.

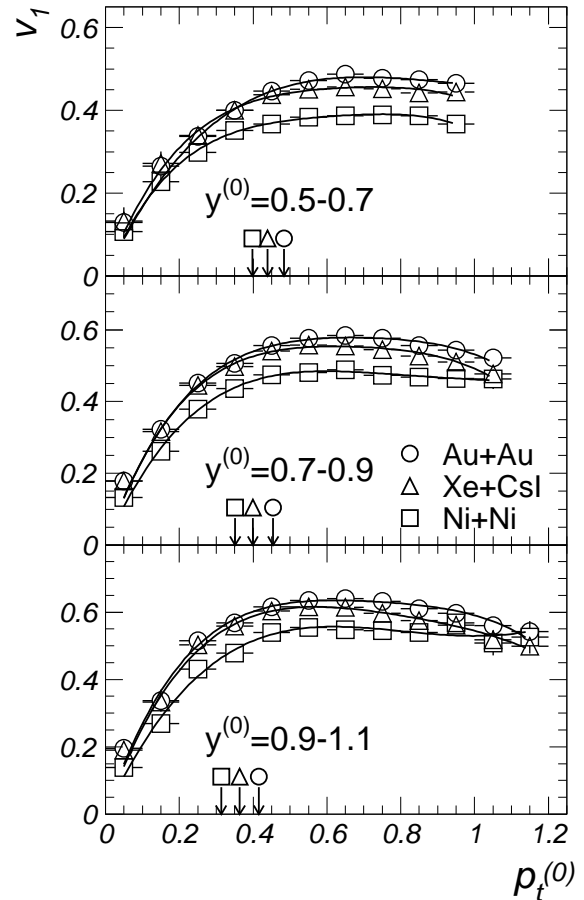


FIG. 9. Differential flow for three systems at 250A MeV, M4 centrality bin, for $Z=2$ particles in three windows of rapidity. The lines are polynomial fits to guide the eye. The arrows mark the values of the average $p_t^{(0)}$ for the corresponding system.

The $(A_P^{1/3} + A_T^{1/3})$ scaling has been proposed by Lang et al. [34], who, within a BUU model, have found a linear dependence of the transverse pressure (leading to transverse momentum transfer) with the reaction time (passage time). Westfall et al. [14] have related the $A^{-1/3}$ dependence of E_{bal} to a competition between the attractive mean field (associated with the surface, so scaling with $A^{2/3}$) and the repulsive nucleon-nucleon interaction (scaling as A). This competition between the two components

may be the origin of the quoted scaling of the transverse pressure with $(A_P^{1/3} + A_T^{1/3})$. Earlier studies devoted to the slope of $\langle p_x \rangle - y$ distributions (which translates into a flow angle) have experimentally confirmed such a scaling [18,22]. We note that, in an ideal hydrodynamics the flow angle is a pure geometric quantity and does not depend on the system size [56]. The system size dependences presented above may be an interesting effect of the nuclear forces and/or a consequence of the non-equilibrium nature of the heavy-ion collisions.

In Fig. 9 we present the differential flow for the three systems at 250A MeV, M4 centrality bin, for $Z=2$ particles in three windows of rapidity (the three panels). The arrows mark the values of the average $p_t^{(0)}$ for the corresponding centrality bin, according to the symbols. For this incident energy of 250A MeV the value of the projectile momentum in the c.m. system is 342 MeV/c per nucleon. As seen already in Fig. 7, for all rapidity windows the $\langle p_t^{(0)} \rangle$ depend on the system size (again breaking the scaling expected from hydrodynamics), suggesting an increase of the compression and expansion with the system size.

Similar data as those presented in Fig. 8 and 9 are presented in the Appendix for $Z=1$ particles at 250A MeV and for $Z=1$ and $Z=2$ particles at 400A MeV (Fig. 25 to Fig. 30).

IV. MODEL COMPARISON

The IQMD transport model [33,41] is widely used for interpreting the data in our energy domain [33,16,20,39]. We use two different parametrizations of the EoS, a hard EoS (compressibility $K=380$ MeV) and a soft EoS ($K=200$ MeV), both with MDI, labeled HM and SM, respectively and without MDI - H and S, respectively. We use the free nucleon-nucleon cross section, σ_{nn}^{free} for all cases, but for the energy of 90A MeV in addition we consider the case of $\sigma_{nn} = 0.8\sigma_{nn}^{free}$. The events produced by the model are filtered by the experimental filter and analyzed in a similar way as the experimental data. This comprises the same recipe for the centrality selection and the same way of reaction plane reconstruction and correction. However, for the energy of 90A MeV, due to a weak flow signal (see below) we prefer to use the true reaction plane for the model calculations. In what concerns the reaction plane resolution at 400A MeV, it is in the model very similar compared to data. For instance, for M4 centrality bin, for IQMD SM the correction factors are 1.03, 1.05 and 1.24 for Au, Xe and Ni systems, respectively.

A. What to compare

A known problem of the IQMD model (and QMD models in general) is that of much lower yields of compos-

ite fragments compared to data [57]. For instance, for Au+Au at incident energy of 400A MeV, M4 centrality, integrated $Z=2$ yields relative to $Z=1$ are 1/4.7 for the experimental data while IQMD predicts 1/25 for HM and 1/15 for SM (these ratios do not depend on including MDI or not).

As cluster formation and flow are intimately related, one cannot simply neglect this dramatic discrepancy. It is difficult to assess whether this strong dependence of fragment production on EoS parametrization is a genuine physical effect or is only particular to IQMD model. We note that most of the present models used in heavy-ion collisions at our energies involve a rather simple phase space coalescence mechanism to produce composite particles [43,49] (IQMD uses the coalescence in coordinate space only [33]). Efforts to identify the fragments early in the collision might contribute to clarify this aspect [58]. Promising theoretical candidates to accomplish the task of realistic fragment formation could be AMD-type models [37].

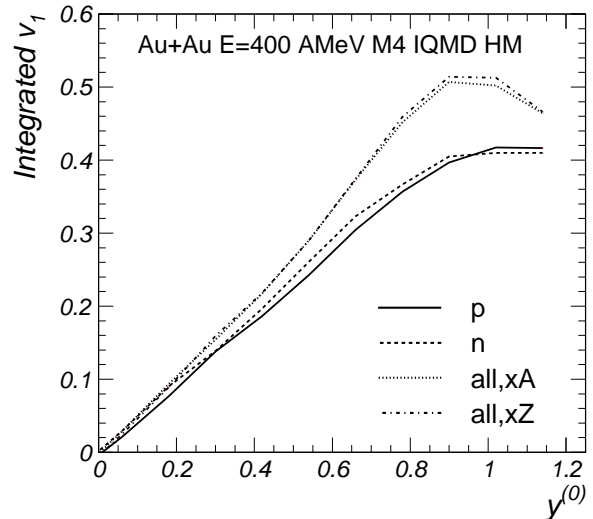


FIG. 10. Comparison of integrated v_1 values as a function of rapidity for protons, neutrons, all particles weighted by mass (A) and all particles weighted by charge (Z) for IQMD HM events, for Au+Au at 400A MeV, M4 centrality.

To partially overcome the problem of fragment production in the models, one can perform the comparison taking into account all charged particles weighted by charge Z (so called proton-likes) [15,20]. However, this type of comparison could be biased, as the neutrons bound in the composite fragments may contribute differently for the calculations compared to data. We have investigated various possibilities by using IQMD events. The results are presented in Fig. 10, where we compare integrated v_1 values as a function of rapidity for protons, neutrons, all particles weighted by mass (A) and all particles weighted by charge (Z) for Au+Au at 400A MeV, M4 centrality bin.

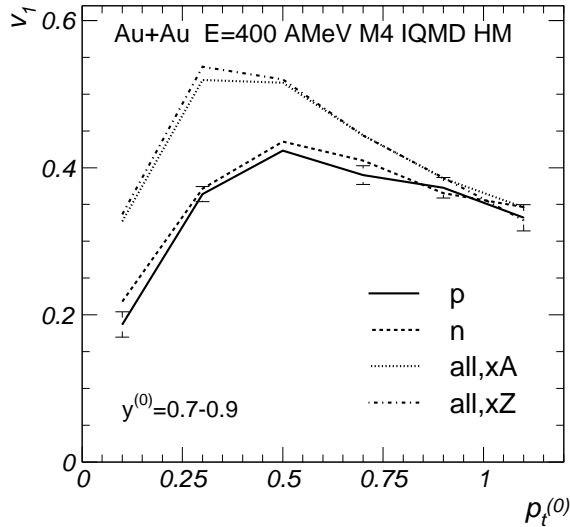


FIG. 11. As Fig. 10, but for differential flow, in the rapidity window $y^{(0)}=0.7-0.9$. The statistical errors are plotted for protons.

In Fig. 11 we show the same comparison in case of differential flow. The neutrons exhibit the same flow as the protons, both for integrated and for differential values. As a consequence, within the model, in both cases the charge-weighted values are identical to the mass-weighted ones. However, as fragments heavier than $Z=2$ are extremely few in the model, this result may be somewhat biased. In the following we are comparing data and model both for selected particle types and for proton-like.

B. Integrated values

We start our comparison of the data with the IQMD model at the incident energy of 90A MeV, for the M4 centrality bin.

In Fig. 12 we show the rapidity dependence of the integrated v_1 values for particles with $Z=1$ (upper panel) and $Z=2$ (lower panel). For both species the measured values are compared to the IQMD calculations for HM and SM parametrizations. For the HM case an additional set of calculations has been performed using $\sigma_{nn} = 0.8\sigma_{nn}^{free}$ (labeled HM.8 in Fig. 12). For the HM case the statistical errors are plotted. For the other cases the errors are comparable. For data the errors are in most cases smaller than the dimension of the points. The calculated values of the directed flow depend both on the parametrized EoS and, more pronounced, on σ_{nn} . This dependence is apparently of different magnitude for $Z=1$ and $Z=2$ particles.

For the model calculations there is a coexistence of attractive (negative v_1 values) and repulsive (positive v_1) flow, manifested as a function of rapidity (we shall call

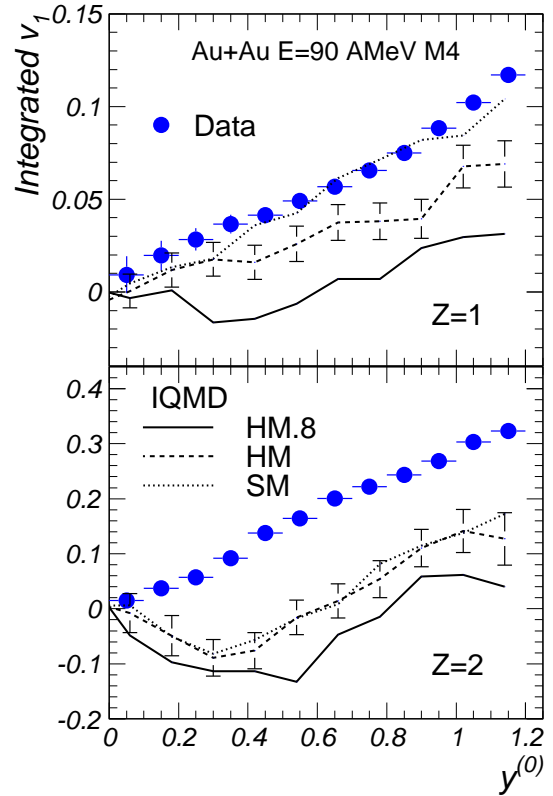


FIG. 12. Integrated v_1 values as a function of rapidity for $Z=1$ and $Z=2$ particles, for the incident energy of 90A MeV. The data points (dots) are compared to IQMD calculations for two EoS (lines) parametrizations. The line labeled HM.8 corresponds to HM case, using $\sigma_{nn} = 0.8\sigma_{nn}^{free}$. For the HM case the statistical errors of the model are plotted.

this dual flow). This coexistence is different for the two particle species. We noticed that the above characteristics of the model calculations depend on centrality as well, both the magnitude of the dual flow and the particle dependence being enhanced for more peripheral collisions. The model features are clearly not supported by the data, which show a monotonic repulsive flow over all the rapidity domain, both for $Z=1$ and $Z=2$ particles, as seen in Fig. 12. For the experimental data, for the centrality M4 studied here, the reaction plane correction factor is 1.54.

A two-component flow was observed earlier in QMD calculations of semi-peripheral Ca+Ca collisions at 350A MeV [39]. That study pointed out its high sensitivity to MDI. But, unless the discrepancy between the calculations and the measured data is resolved, any conclusion on the sensitivity of the directed flow on the EoS, σ_{nn} or MDI is meaningless for energies around E_{bal} . It is not clear for the moment whether the particle dependence of the dual flow is not an artifact of the treatment of composite particles in the model. We note that measurements of E_{bal} for different particle types [14,23] did not reveal, so far, any dual flow. Calculations with a

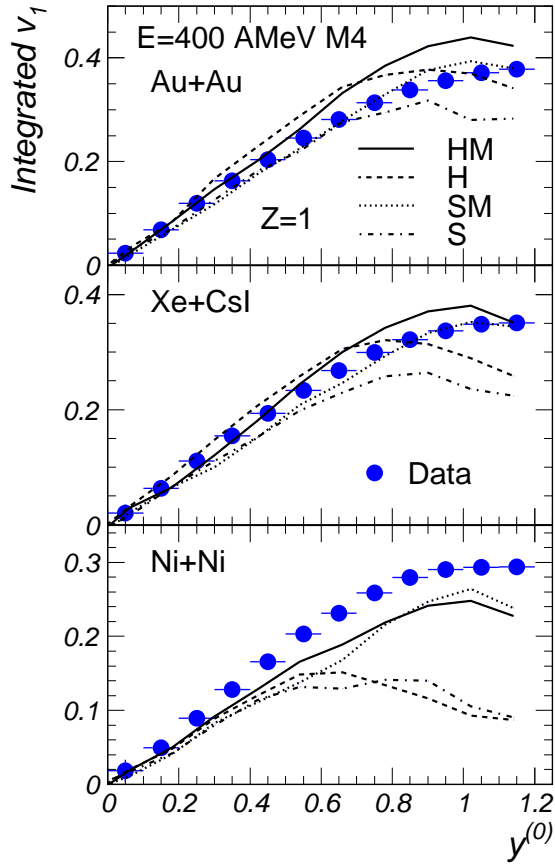


FIG. 13. Integrated v_1 values as a function of rapidity, for $Z=1$ particles, for three systems at 400A MeV, centrality bin M4. The data points (dots) are compared to IQMD calculations (lines).

BUU model [44] found a dual flow only in a (p_t) differential way, but otherwise monotonic behavior of $\langle p_x \rangle - y$ distributions. Recent experimental investigations of flow in light systems at E_{bal} pointed out interesting aspects of flow of light isotopes and heavy fragments, but again the balance energy was found not to depend on particle type [59].

In Fig. 13 and Fig. 14 we show the comparison of data and model calculations for $Z=1$ and $Z=2$ particles, respectively. The three studied systems are considered, for the centrality bin M4. The integrated v_1 values show sensitivity to both EoS and to MDI. As expected, the MDI influence the flow essentially in the vicinity of the projectile spectator ($y^{(0)} > 0.8$). This effect is more pronounced the lighter the system. All these sensitivities are enhanced for $Z=2$ particles. For Au+Au and Xe+CsI systems, the SM parametrization is reproducing the data very well, for both $Z=1$ and $Z=2$ particles. This may be the result of a similar balance of thermal and collective contributions in the model compared to the data. In fact, the phase space populations of $Z=1$ and $Z=2$ particles are similar for model and data.

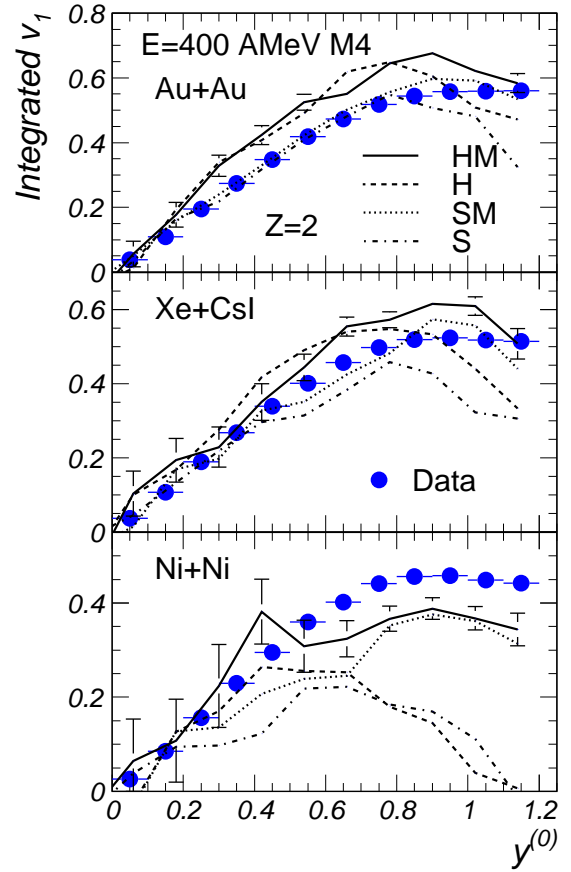


FIG. 14. As Fig. 13, but for $Z=2$ particles. For the HM case the statistical errors of the model are plotted.

In case of Ni+Ni system the dependence on EoS is already negligible, but obviously the model underestimates the flow. One parameter of the model, the Gaussian width L , which is the phase space extension of the wave packet of the particle (and acting as an effective interaction range) has been found to influence the directed flow considerably [41]. A decrease of L for lighter systems has been advocated with the argument of maximum stability of nucleonic density profiles [41]. As no clear prescription exists for handling the value of L , we prefer to use a constant value of $L=8.66 \text{ fm}^2$ throughout the present work. A smaller L would lead to an increase of the directed flow [41] and may cure the discrepancy that we observe for the Ni+Ni system, but will affect unfavorably the comparison in case of Xe+CsI system. These effects may reflect the importance played (via the interaction range) by the surface. A complete understanding of this aspect is a necessary step towards establishing the bulk properties of the nuclear matter created in heavy-ion collisions.

We note that comparisons of integrated directed flow for Au+Au system using QMD-type models favored mostly a soft EoS [15,54] but a hard EoS was also found to explain another set of experimental data [16].

In Fig. 15 we present the comparison of the measured

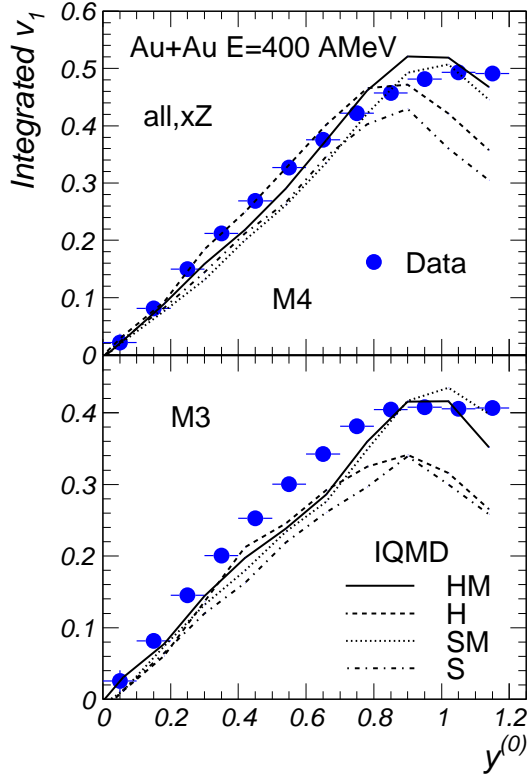


FIG. 15. Integrated v_1 values as a function of rapidity for all particles weighted by Z , for the centrality bins M4 (upper panel) and M3 (lower panel), for the incident energy of 400A MeV. The data points (dots) are compared to IQMD calculations (lines).

integrated v_1 values to IQMD calculations for Au+Au at the incident energy of 400A MeV, taking into account all charged particles weighted by charge Z . The centrality bins M4 and M3 are studied. In this case the sensitivity to EoS is reduced, as a consequence of a balance between magnitude of flow and yield of composite particles in the model: hard EoS produces more flow, but less particles with $Z > 1$, while for soft EoS it is opposite. This behavior strongly underlines once more the necessity that theoretical models appropriately describe the yields of composite particles. The conclusion on EoS is this time less evident, but the parametrizations without MDI are ruled out once again, on the basis of their departure from the data in the region of spectator rapidity. As expected, this effect is more pronounced for the more peripheral centrality bin M3.

Despite the good agreement seen at the beam energy of 400A MeV, we found that in the IQMD model the decrease of flow towards lower incident energies is much faster than for data, leading to larger theoretical E_{bal} compared to data (and to the behavior seen in Fig. 12). This may be a result of deficiencies in incorporating MDI and in the treatment of fragment production. The Pauli blocking may play a role too. In addition, it has been

pointed out that the shape of the flow excitation function is drastically influenced by the method of imposing constraints on the Fermi momenta [41]. The features of the model calculations presented above for 400A MeV show the danger of deriving EoS-related conclusions from rapidity-integrated flow values (like p_x^{dir}) unless a detailed description of the data is first achieved in a differential way. As realized early on [27], a soft EoS with MDI is producing similar magnitude in p_x^{dir} as a hard EoS without MDI.

C. Differential flow

We restrict our model comparison of the differential flow to the incident energy of 400A MeV and M4 centrality bin. Data for all three systems investigated so far are compared to the model calculations.

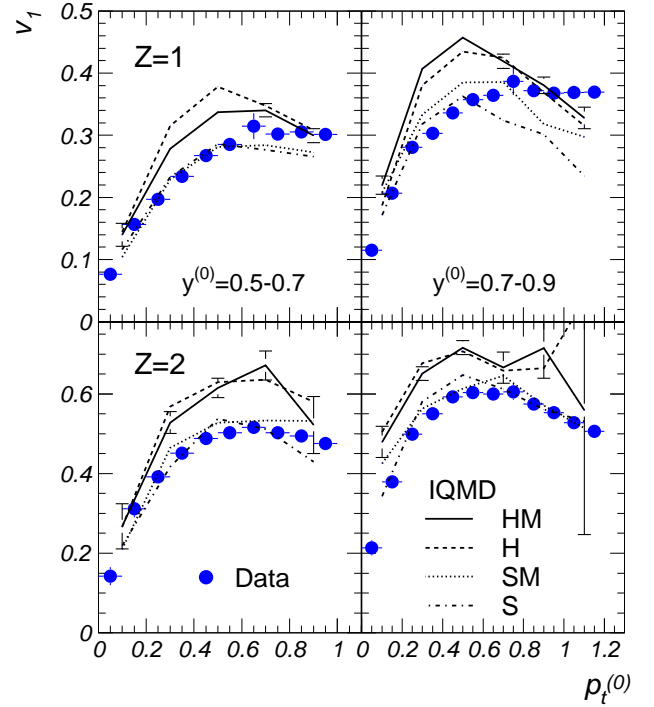


FIG. 16. Differential flow for particles with $Z=1$ (upper row) and $Z=2$ (lower row) for Au+Au collisions at incident energy of 400A MeV, M4 centrality, for two windows in rapidity (columns). Experimental data are represented by dots and the model calculations are the lines. For the HM case the statistical errors of the model are plotted.

In Fig. 16 the measured differential directed flow for Au+Au collisions at incident energy of 400A MeV, M4 centrality, is compared to the IQMD results for all the four parametrizations used above. Particles with $Z=1$ (upper row) and $Z=2$ (lower row) for two windows in rapidity are used for the comparison. For both particle species there is a clear sensitivity of DDF on the EoS. As for the case of the integral flow, the SM parametrization

reproduces the experimental data quite well. Apparently the model calculations deviate from the data at high p_t in case of $Z=1$ particles, while the corresponding $Z=2$ particles are well explained. This deviation is more pronounced for larger rapidities. We have found earlier [60] that a BUU model does not explain the DDF of protons in the spectator region at higher energies. The shape of the $Z=1$ DDF distributions are in case of the IQMD model strikingly similar to the ones of $Z=2$, while for the data there are subtle differences between the two particle species (at this energy of 400A MeV as well as down to 90A MeV [48]). The model features may be the result that the nucleons (dominating the $Z=1$ sample) in the models are all “primordial”, which does not account for the sequential decays of heavier fragments. The dynamics of the expansion and fragment formation may be responsible for the differences, too.

TABLE III. Average normalized transverse momentum $\langle p_t^{(0)} \rangle$ for particles with $Z=1$ and $Z=2$ in Au+Au collisions at 400A MeV, M4 centrality bin. Data and model values are compared for two rapidity windows. For data, the number in parenthesis represents the error on the last digit.

Rapidity, particle	Data	IQMD HM	IQMD SM
$y^{(0)}=0.5-0.7$ $Z=1$	0.60(3)	0.62	0.62
$Z=2$	0.48(2)	0.42	0.44
$y^{(0)}=0.7-0.9$ $Z=1$	0.58(3)	0.55	0.56
$Z=2$	0.44(2)	0.37	0.37

In Table III we compare the experimental values of the average normalized transverse momentum with the values from IQMD, for HM and SM cases. Particles with $Z=1$ and $Z=2$ for the two windows in rapidity studied in Fig. 16 are compared. The data values have a systematic error represented by the number in parenthesis as the error on the last digit. The model reproduces reasonably well the average transverse momenta for $Z=1$ particles, while it underestimates them for $Z=2$, for both windows of rapidity.

We mention that, recently, our experimental differential directed flow in Au+Au [48] was nicely reproduced by a BUU model which includes an improved Dirac-Brueckner formalism [49]. In this case, for the densities expected at 400A MeV, the EoS is soft, which is in agreement to our results.

In Fig. 17 we show the measured DDF for Xe+CsI and Ni+Ni systems at 400A MeV, M4 centrality, in comparison to IQMD results, for $Z=1$ particles in two windows of rapidity. In case of Xe+CsI system the model calculations are at the same level of agreement with data as in case of Au+Au: the SM parametrization is reproducing the data, with clear deviations at high momenta. For the Ni+Ni case even the HM parametrization underpredicts the measured data. Most notably, as obvious particularly for Ni+Ni, the MDI have effects predominantly at low p_t , contrary to earlier BUU predictions (performed for the asymmetric system Ar+Pb) [36].

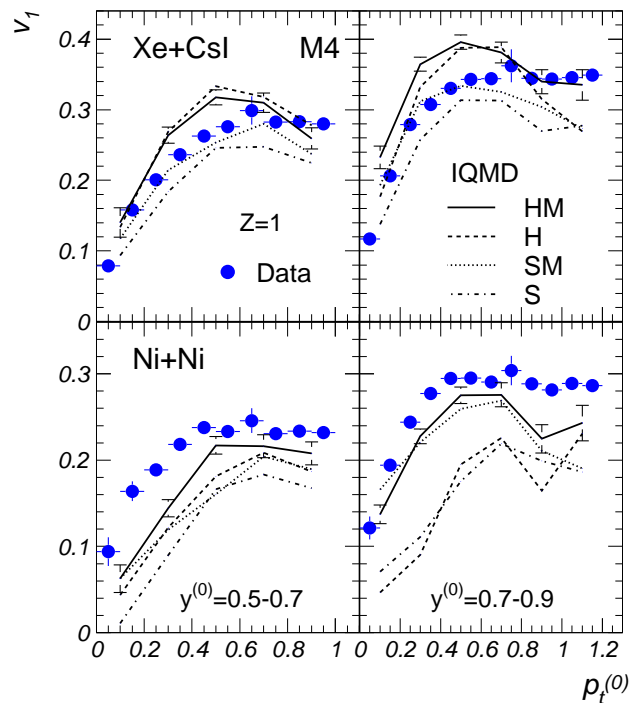


FIG. 17. Comparison of data and model differential flow for $Z=1$ particles, for the incident energy of 400A MeV, M4 centrality bin, for the systems Xe+CsI (upper row) and Ni+Ni (lower row) for two windows in rapidity (columns).

In Fig. 18 we show the model comparison of the differential flow for particles weighted by Z for Au+Au collisions at incident energy of 400A MeV, M4 centrality, for two windows in rapidity. As in case of integrated values, as a result of different relative contribution of particles heavier than $Z=1$, the sensitivity to EoS is reduced for this type of comparison.

V. SUMMARY AND CONCLUSIONS

We have presented experimental results on directed flow in Au+Au, Xe+CsI and Ni+Ni collisions at incident energies from 90 to 400A MeV. General features of the directed flow have been investigated using experimental data, particularly the centrality and the system dependence. We have studied the rapidity dependence of the first Fourier coefficient, v_1 , integrating over all transverse momentum range. A special emphasis has been put on the differential directed flow, namely the p_t dependence of v_1 . While for integrated values we presented a new way of looking at old (and generally known) dependences, the DDF results are reported for the first time for our energy domain, both for the centrality and for the system size dependence. We have devoted special care to the corrections of the experimental data. The influence of the finite granularity of the detector has been studied and corrected for. The high accuracy of the final results is

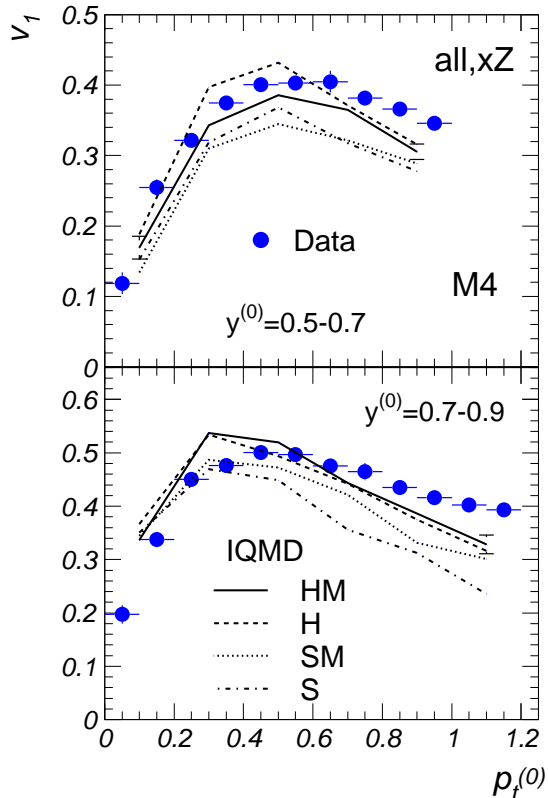


FIG. 18. Differential flow for particles weighted by Z for Au+Au collisions at incident energy of $400A$ MeV, M4 centrality, for two windows in rapidity. Experimental data are represented by dots. The model calculations are the lines.

based as well on a good reaction plane resolution achieved with the full coverage of the FOPI detector.

We have compared the experimental data with IQMD transport model calculations, for both integral and differential v_1 values. This comparison, performed for all the three studied systems, shows a clear sensitivity of the directed flow on the EoS parametrization in the model, especially in case of particle-selected comparison. In this case, for both integrated and differential directed flow at the incident energy of $400A$ MeV, we conclude that a soft EoS with MDI is the only parametrization in the model that reproduces the data for Au and Xe systems. A clear discrepancy is seen for Ni system, which needs to be addressed separately. It may reflect the increasing importance played by the nuclear surface for lighter systems. We consider our present results as a case study on the sensitivities in determination of EoS and MDI from directed flow comparisons. We emphasized the necessity of the present kind of differential comparison prior to more global quantities. We have shown that the combination of rapidity and transverse momentum analysis of (differential) directed flow can impose constraints on the model. We also pointed out some difficulties of the model to reproduce the measured data concerning: i) flow at low energy (we considered here $90A$ MeV), ii) flow as a func-

tion of system size, and iii) fragment production. As a consequence, none of the IQMD parametrizations studied here is able to consistently explain the whole set of experimental data.

The importance of spectators acting as clocks for the expansion is one particular argument to study collective flow in semi-central collisions at energies from a few hundred MeV to a few GeV per nucleon [4]. We have demonstrated that high precision experimental data allows us to study the many facets of the heavy-ion collisions. Other observables, like v_2 , should receive a comparable (and simultaneous) attention too. Whether the nuclear equation of state can be extracted from such studies depends ultimately on the ability of any type of microscopic transport model to reproduce the measured features.

ACKNOWLEDGMENT

This work has been supported in part by the German BMBF under contracts 06HD953, RUM-005-95/RUM-99/010, POL-119-95, UNG-021-96 and RUS-676-98 and by the Deutsche Forschungsgemeinschaft (DFG) under projects 436 RUM-113/10/0, 436 RUS-113/143/2 and 446 KOR-113/76/0. Support has also been received from the Polish State Committee of Scientific Research, KBN, from the Hungarian OTKA under grant T029379, from the Korea Research Foundation under grant No. KRF-2002-015-CS0009, from the agreement between GSI and CEA/IN2P3 and from the PROCOPE Program of DAAD.

APPENDIX

In the following we present additional results that complement those included in the body of the paper. As the trends are similar to those already discussed in section III, we present here only figures.

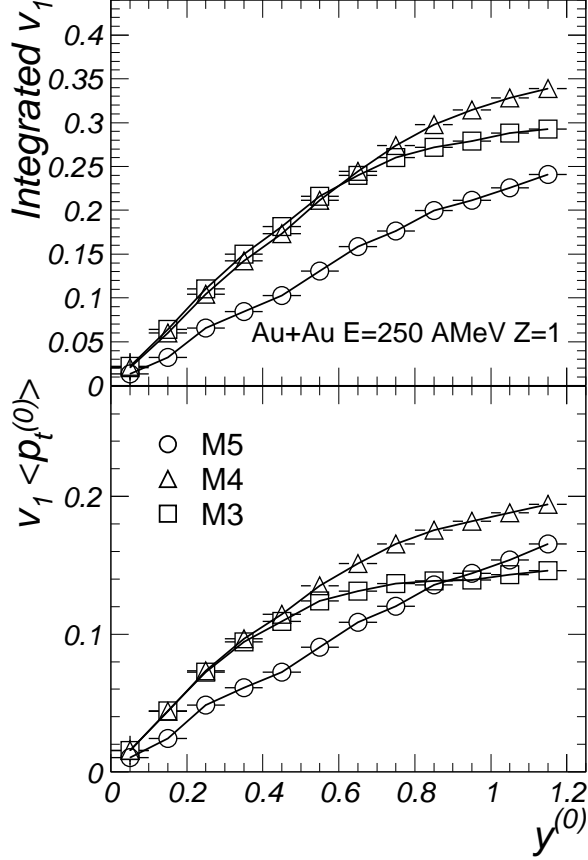


FIG. 19. Centrality dependence of the integrated directed flow as a function of rapidity for Au+Au at 250A MeV for $Z=1$ particles.

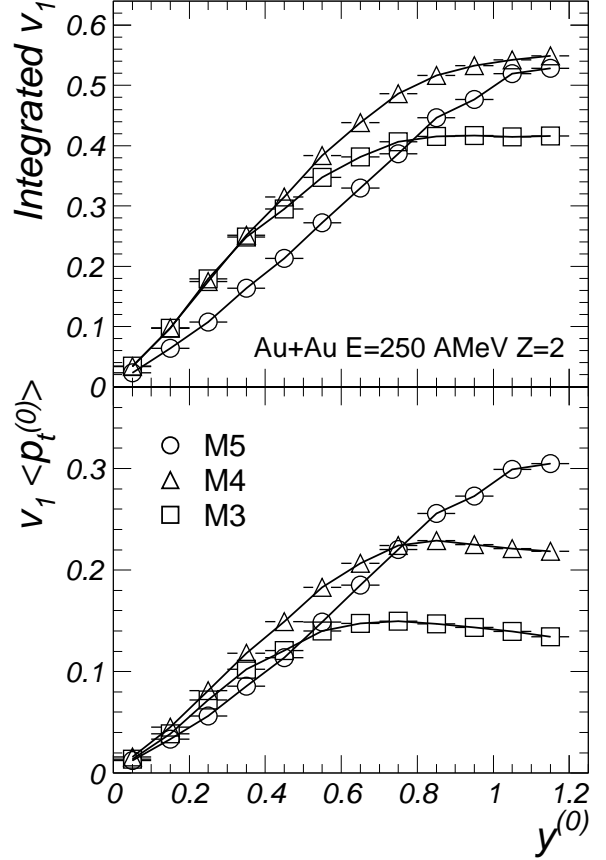


FIG. 20. Centrality dependence of the integrated directed flow as a function of rapidity for Au+Au at 250A MeV for $Z=2$ particles.

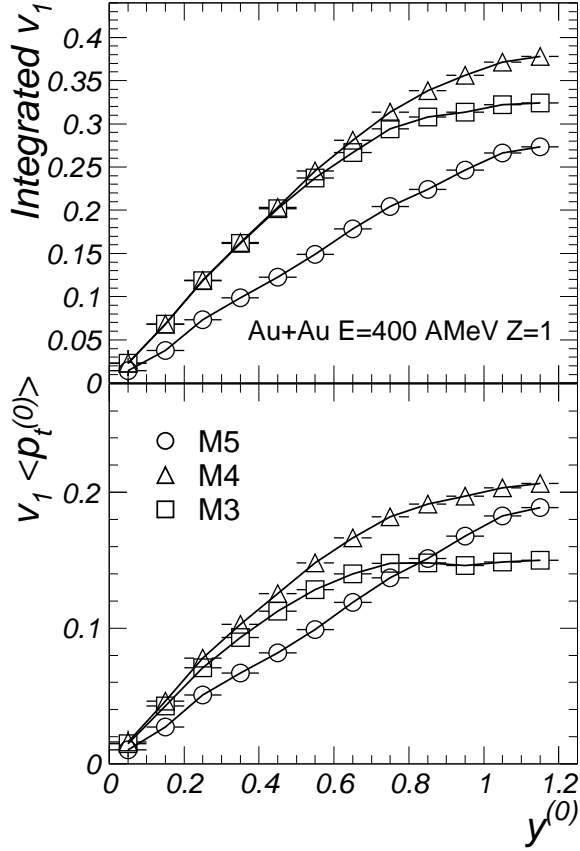


FIG. 21. Centrality dependence of the integrated directed flow as a function of rapidity for Au+Au at 400A MeV for $Z=1$ particles.

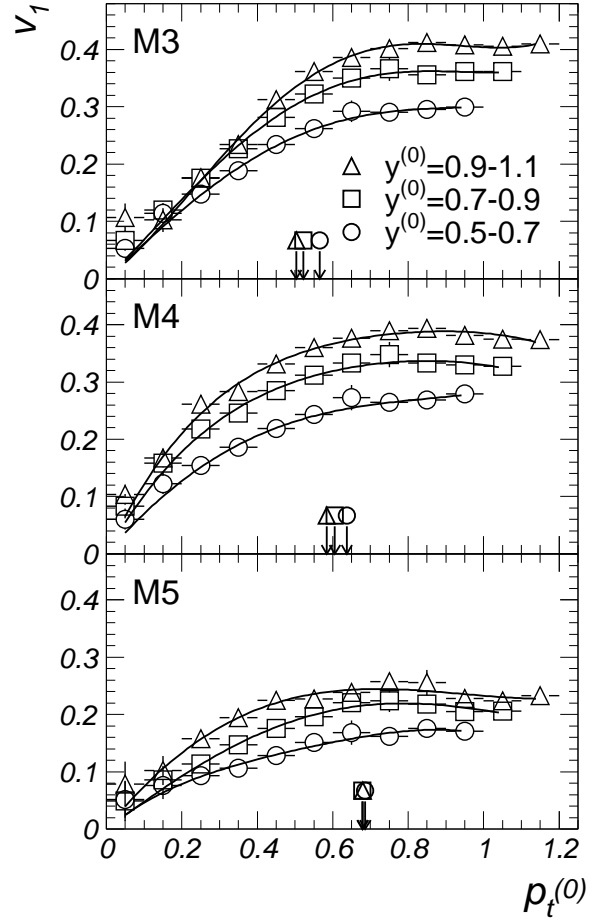


FIG. 22. Differential flow for three centrality bins, in three rapidity windows, for $Z=1$ particles for collisions Au+Au at 250A MeV. The lines are polynomial fits to guide the eye. The arrows mark the values of the average $p_t^{(0)}$ for the corresponding centrality bin.

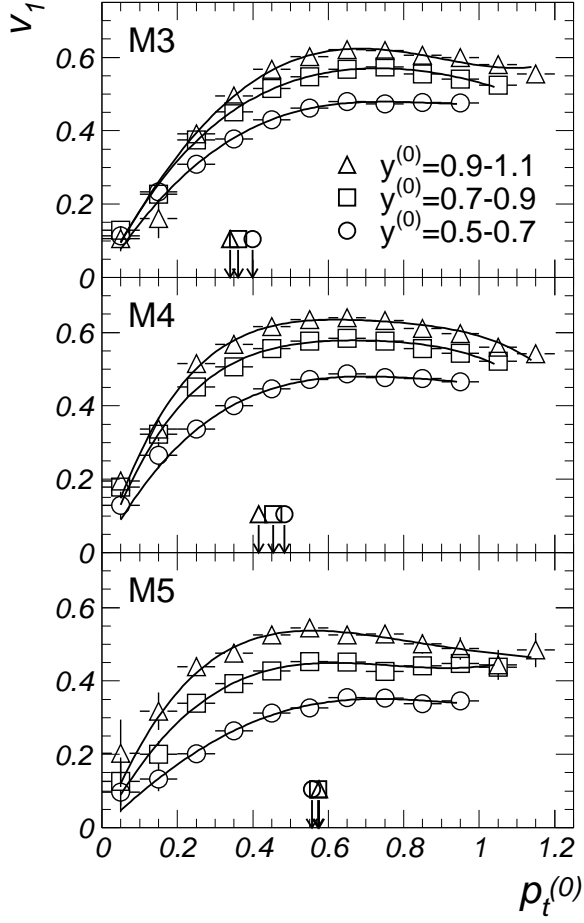


FIG. 23. Differential flow for three centrality bins, in three rapidity windows, for $Z=2$ particles for collisions Au+Au at 250A MeV.

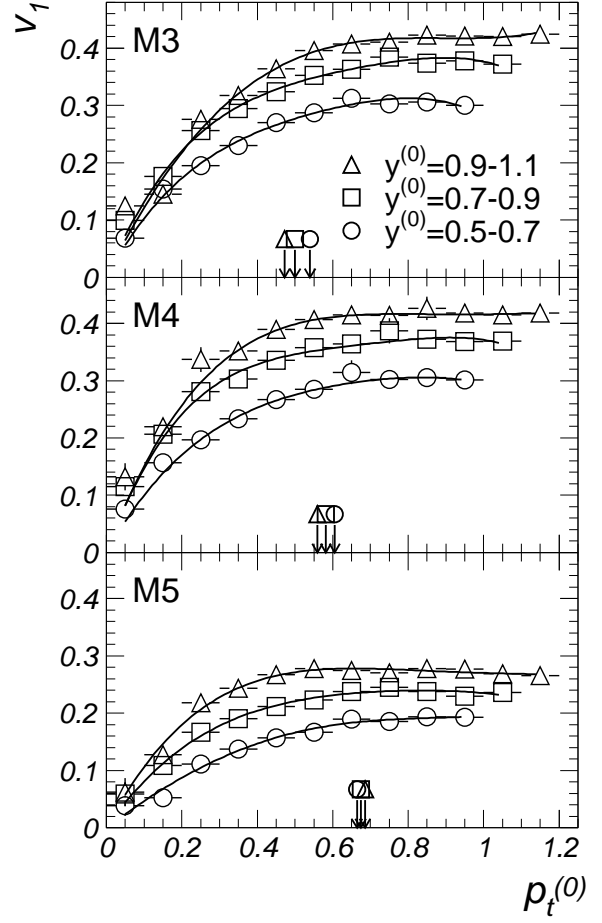


FIG. 24. Differential flow for three centrality bins, in three rapidity windows, for $Z=1$ particles for collisions Au+Au at 400A MeV.

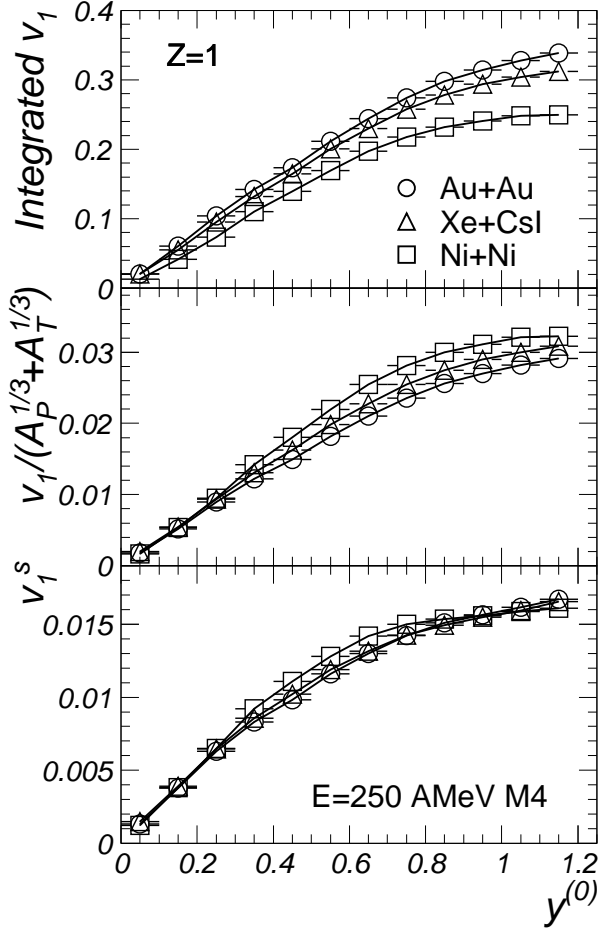


FIG. 25. Integrated directed flow as a function of rapidity for $Z=1$ particles in the M4 centrality bin of collisions Au+Au, Xe+CsI and Ni+Ni at 250A MeV. Upper panel: v_1 values, middle panel: v_1 scaled by the term $(A_P^{1/3} + A_T^{1/3})$, lower panel: scaled values, $v_1^s = v_1 \langle p_t^{(0)} \rangle / (A_P^{1/3} + A_T^{1/3})$.

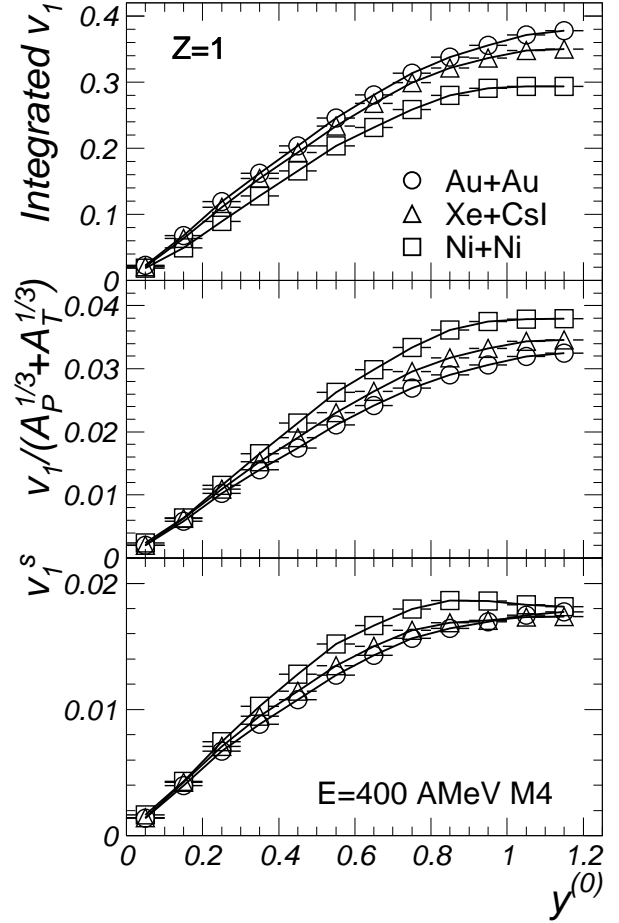


FIG. 26. Integrated directed flow as a function of rapidity for $Z=1$ particles in the M4 centrality bin of collisions Au+Au, Xe+CsI and Ni+Ni at 400A MeV.

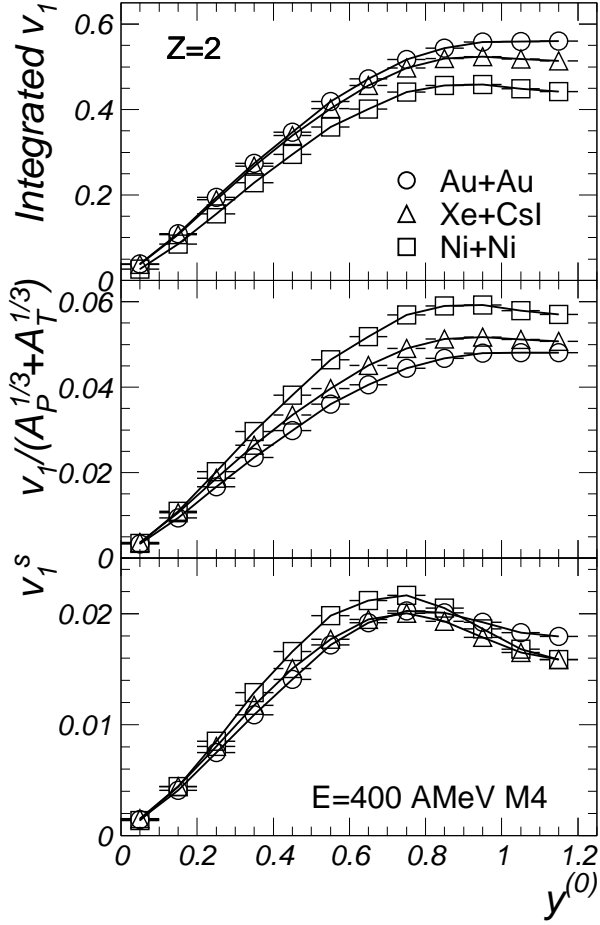


FIG. 27. Integrated directed flow as a function of rapidity for $Z=2$ particles in the M4 centrality bin of collisions Au+Au, Xe+CsI and Ni+Ni at 400A MeV.

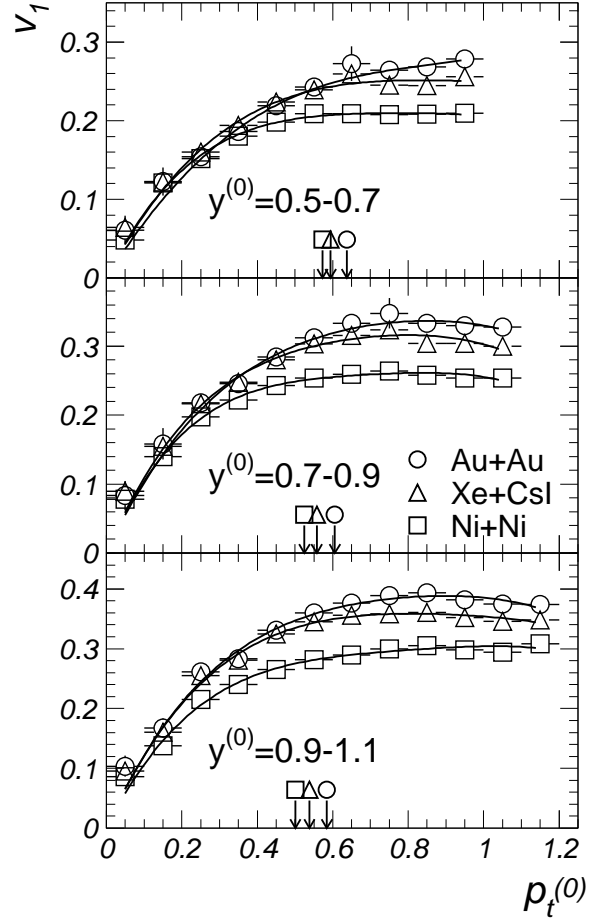


FIG. 28. Differential flow for three systems at 250A MeV, M4 centrality bin, for $Z=1$ particles in three windows of rapidity. The lines are polynomial fits to guide the eye. The arrows mark the values of the average $p_t^{(0)}$ for the corresponding system.

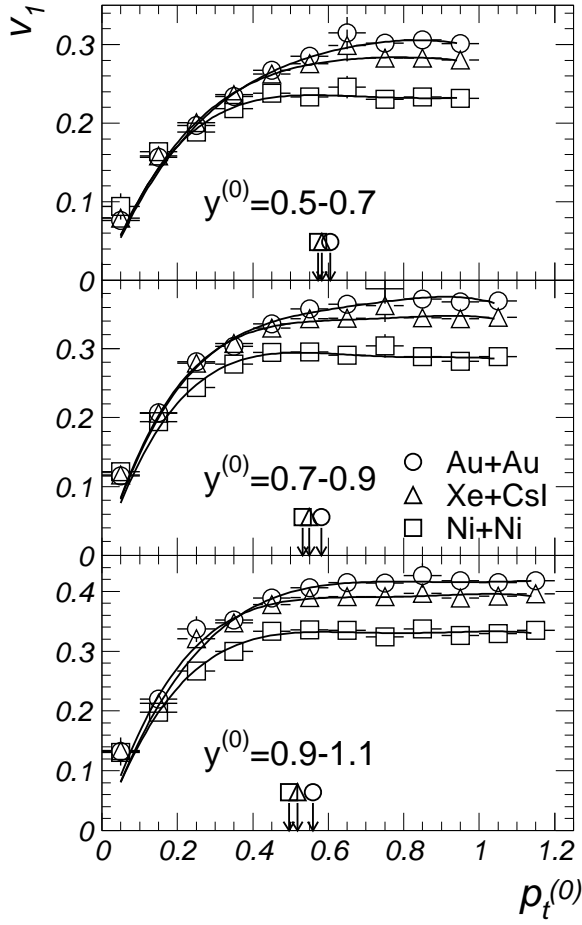


FIG. 29. Differential flow for three systems at 400A MeV, M4 centrality bin, for $Z=1$ particles in three windows of rapidity.

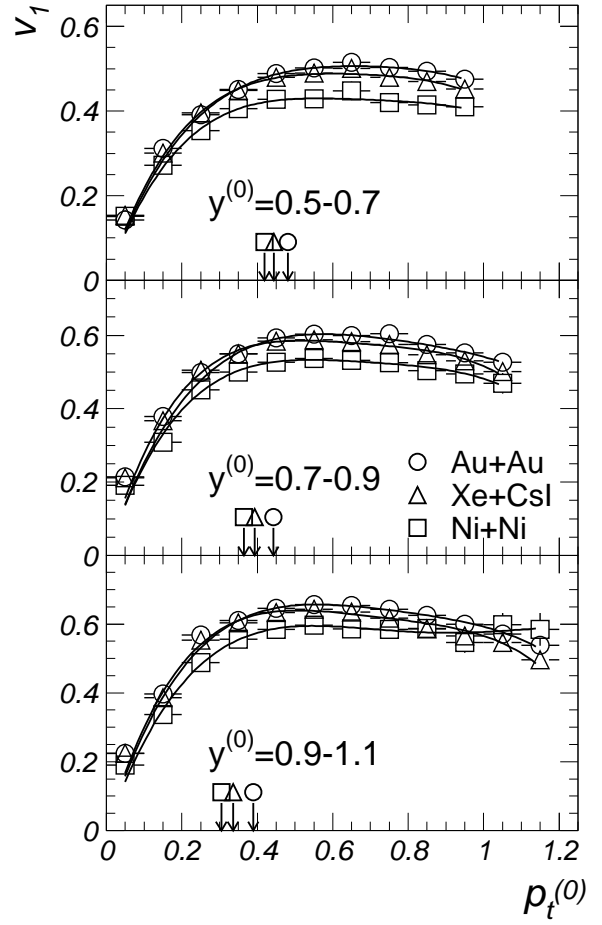


FIG. 30. Differential flow for three systems at 400A MeV, M4 centrality bin, for $Z=2$ particles in three windows of rapidity.

-
- [1] W. Reisdorf and H.G. Ritter, *Ann. Rev. Nucl. Part. Sc.* **47**, 663 (1997).
- [2] N. Herrmann, J.P. Wessels, and T. Wienold, *Ann. Rev. Nucl. Part. Sc.* **49**, 581 (1999).
- [3] H. Stöcker and W. Greiner, *Phys. Rep.* **137**, 277 (1986).
- [4] P. Danielewicz, *Nucl. Phys. A* **685**, 368c (2001) [nucl-th/0112006]; nucl-th/0112006; nucl-th/0201032.
- [5] H. Stöcker, J.A. Maruhn, and W. Greiner, *Phys. Rev. Lett.* **44**, 725 (1980).
- [6] H.A. Gustafsson et al., *Phys. Rev. Lett.* **52**, 1590 (1984).
- [7] R.E. Renfordt et al., *Phys. Rev. Lett.* **53**, 763 (1984).
- [8] P. Danielewicz and G. Odyniec, *Phys. Lett. B* **157**, 146 (1985).
- [9] K.G.R. Doss et al., *Phys. Rev. Lett.* **57**, 302 (1986).
- [10] K.G.R. Doss et al., *Phys. Rev. Lett.* **59**, 2720 (1987).
- [11] D. Keane et al., *Phys. Rev. C* **37**, 1447 (1988).
- [12] C. Ogilvie et al., *Phys. Rev. C* **40**, 2592 (1989).
- [13] W.M. Zhang et al., *Phys. Rev. C* **42**, R491 (1990).
- [14] G.D. Westfall et al., *Phys. Rev. Lett.* **71**, 1986 (1993).
- [15] V. Ramillien et al., *Nucl. Phys. A* **587**, 802 (1995).
- [16] M.D. Partlan et al., *Phys. Rev. Lett.* **75**, 2100 (1995).
- [17] M.J. Huang et al., *Phys. Rev. Lett.* **77**, 3739 (1996).
- [18] J. Chance et al., *Phys. Rev. Lett.* **78**, 2535 (1997).
- [19] P. Crochet et al., *Nucl. Phys. A* **624**, 725 (1997).
- [20] P. Crochet et al., *Nucl. Phys. A* **627**, 522 (1997).
- [21] R. Pak et al., *Phys. Rev. Lett.* **78**, 1022 (1997); R. Pak et al., *Phys. Rev. Lett.* **78**, 1026 (1997).
- [22] F. Rami et al., *Nucl. Phys. A* **646**, 367 (1999).
- [23] D.J. Magestro et al., *Phys. Rev. C* **61**, 021602(R) (2000).
- [24] H. Liu et al., *Phys. Rev. Lett.* **84**, 5488 (2000).
- [25] J. Kapusta and D. Strottman, *Phys. Lett. B* **106**, 33 (1981).
- [26] J.J. Molitoris, J.B. Hoffer, H. Kruse, and H. Stöcker, *Phys. Rev. Lett.* **53**, 899 (1984).
- [27] J. Aichelin, A. Rosenhauer, G. Peilert, H. Stöcker, and W. Greiner, *Phys. Rev. Lett.* **58**, 1926 (1987).
- [28] A. Bonasera and L.P. Csernai, *Phys. Rev. Lett.* **59**, 630 (1987).
- [29] G. Peilert, H. Stöcker, W. Greiner, A. Rosenhauer, A. Bohnet, and J. Aichelin, *Phys. Rev. C* **39**, 1402 (1989).
- [30] V. Koch, B. Blättel, W. Cassing, U. Mosel, and K. Weber, *Phys. Lett. B* **241**, 174 (1990).
- [31] C. Gale, G.M. Welke, M. Prakash, S.J. Lee, and S. Das Gupta, *Phys. Rev. C* **41**, 1545 (1990).
- [32] B. Blättel, V. Koch, A. Lang, K. Weber, W. Cassing, and U. Mosel, *Phys. Rev. C* **43**, 2728 (1991).
- [33] J. Aichelin, *Phys. Rep.* **202**, 233 (1991).
- [34] A. Lang, B. Blättel, W. Cassing, V. Koch, U. Mosel, and K. Weber, *Z. Phys. A* **340**, 287 (1991).
- [35] J. Jaenicke, J. Aichelin, H. Ohtsuka, R. Linden, and A. Faessler, *Nucl. Phys. A* **536**, 201 (1992).
- [36] Q. Pan and P. Danielewicz, *Phys. Rev. Lett.* **70**, 2062 (1993); *Phys. Rev. Lett.* **70**, 3523 (1993).
- [37] A. Ono, H. Horiuchi, and T. Maruyama, *Phys. Rev. C* **48**, 2946 (1993).
- [38] A. Insolia, U. Lombardo, N.G. Sandulescu, and A. Bonasera, *Phys. Lett. B* **334**, 12 (1994).
- [39] S. Soff, S.A. Bass, C. Hartnack, H. Stöcker, and W. Greiner, *Phys. Rev. C* **51**, 3320 (1995).
- [40] C. Fuchs, T. Gaitanos, and H.H. Wolter, *Phys. Lett. B* **381**, 23 (1996).
- [41] C. Hartnack, R.K. Puri, J. Aichelin, J. Konopka, S.A. Bass, H. Stöcker, and W. Greiner, *Eur. J. Phys. A* **1**, 151 (1998).
- [42] P.K. Sahu et al., *Nucl. Phys. A* **640**, 493 (1998).
- [43] A. Insolia, U. Lombardo, and N. Sandulescu, *Phys. Rev. C* **61**, 067902 (2000).
- [44] B.-A. Li and A. Sustich, *Phys. Rev. Lett.* **82**, 5004 (1999).
- [45] J. Barette et al., *Phys. Rev. C* **59**, 884 (1999).
- [46] B.-A. Li, C.M. Ko, and G.Q. Li, *Phys. Rev. C* **54**, 844 (1996).
- [47] S. Voloshin, *Phys. Rev. C* **55**, R1630 (1997).
- [48] A. Andronic et al., *Phys. Rev. C* **64**, 041604(R) (2001) [nucl-ex/0108014].
- [49] T. Gaitanos, C. Fuchs, H.H. Wolter, and A. Faessler, *Eur. J. Phys. A* **12**, 421 (2001) [nucl-th/0102010].
- [50] A. Gobbi et al., *Nucl. Instr. and Meth. in Phys. Res. A* **324**, 156 (1993); J. Ritman for the FOPI Collaboration, *Nucl. Phys. B (Proc. Suppl.)* **44** (1995) 708.
- [51] A. Andronic et al., *Nucl. Phys. A* **679**, 765 (2001).
- [52] J.-Y. Ollitrault, nucl-ex/9711003.
- [53] N. Borghini, P.M. Dinh, and J.-Y. Ollitrault, *Phys. Rev. C* **64**, 054901 (2001) [nucl-th/0105040]; N. Borghini, P.M. Dinh, J.-Y. Ollitrault, A.M. Poskanzer, and S.A. Voloshin, nucl-th/0202013; N. Borghini, P.M. Dinh, and J.-Y. Ollitrault, nucl-th/0204017.
- [54] P. Crochet, PhD Thesis, Strasbourg, CRN 96-09 (1996).
- [55] GEANT – Detector Description and Simulation Tool, CERN Program Library Long Writeup W5013; http://wwwinfo.cern.ch/asdoc/geant_html3/geantall.html.
- [56] W. Schmidt, U. Katscher, B. Waldhauser, J.A. Maruhn, H. Stöcker, and W. Greiner, *Phys. Rev. C* **47**, 2782 (1993).
- [57] W. Reisdorf et al., *Nucl. Phys. A* **612**, 493 (1997).
- [58] R.K. Puri, C. Hartnack, and J. Aichelin, *Phys. Rev. C* **54**, R28 (1996).
- [59] D. Cussol et al., *Phys. Rev. C* **65**, 044604 (2002).
- [60] P. Crochet et al., *Phys. Lett. B* **486**, 6 (2000) [nucl-ex/0006004].